How the Anatomy of the Epidermal Cells Is Correlated to the Transient Response of Stomata

Maryam Alsadat Zekri *[1], Daniel Tholen[2], Lukas Koller[2], Ingeborg Lang[1], Guillaume Theroux-Rancourt [2,3]

[1] Department of Functional and Evolutionary Ecology, Faculty of Life Sciences, University of Vienna, Djerassiplatz 1, A-1030, Vienna, Austria

[2] Department of Integrative Biology and Biodiversity Research, Institute of Botany, University of Natural Resources and Life Sciences, Gregor-Mendel-Straße 33, A-1180, Vienna, Austria

[3] Biopterre – Bioproducts development center, Indoor farming department, 1642, rue de la Ferme, Sainte-Anne-de-la-Pocatière (Québec), G0R 1Z0, Canada

*Corresponding author: Maryam.Alsadat.Zekri@univie.ac.at

Abstract

Here, we show the possible correlation between the anatomical characteristics of epidermal cells of *Arabidopsis thaliana* with the stomata transient opening, which is commonly called the Wrong-Way Response (WWR). The WWR was induced by either reduced air humidity or leaf excision. Five genotypes of *A. thaliana* Col8, *epf1epf2*, *lcd1-1*, SALK069, and UBP, respectively, with anatomical differences in epidermal cells such as stomatal density, stomata size, size, and shape of the pavement cells were selected. These genotypes allowed us to investigate the mutual effects of stomata density and size on WWR. Scanning Electron Microscopy (SEM) was applied for image acquisition of the abaxial and adaxial surface of the leaves and the main features of the epidermal cells were extracted by one of the additions to the MiToBo plugin of ImageJ/Fiji called PaCeQuant. The stomatal conductance to water vapor (g_s) was measured using the portable photosynthesis measurement system LICor-6800. Our linear models showed that the size of the stomata explained the rate of WWR induced by reduced air humidity, so genotypes with smaller stomata showed a smaller rate of the WWR. After leaf excision, however, there was no correlation between the size of the stomata and the rate of the WWR. Moreover, we found that after both, reduced air humidity and leaf excision, the size of the pavement cells on the abaxial surface is correlated to the rate of the WWR; genotypes with smaller pavement cells on the abaxial surface had a smaller rate of WWR.

Key words: stomata, pavement cells, Wrong-Way Response (WWR), *Arabidopsis thaliana*, leaf anatomy

Introduction

Stomata are tiny pores on the leaf surface that function as gatekeepers between the atmosphere and the leaf interior, regulating the intake of CO_2 and limiting transpiration. Stomata are very sensitive to environmental conditions that change the water potential of the plant (e.g., through soil drought or through a decline in air humidity). Yet, there are standing questions about how stomata respond to the surrounding environment, because the movement of stomata is not in response to a single factor (Merilo et al., 2014). The closure of stomata has been explained as a hydroactive feedback caused by accumulation of abscisic acid (ABA), a process through which osmotic solutes are released from the guard cells. Consequently, the relaxation by reduction of osmotic pressure leads to the closure of stomata (Bharath et al., 2021, Buckley, 2019). On the other hand, a transient opening of stomata after reducing the water supply is often observed, either after leaf excision (Darwin, 1898, Buckley et al., 2011) or after a reduction in humidity of the air surrounding the leaf (Buckley, 2019, Buckley et al., 2011). This phenomenon is named the Wrong-Way Response (WWR) and is considered a hydropassive feedback originating from a reduction of epidermal turgor pressure, which allows the turgid guard cells to pull apart from each other and results in stomatal opening (Buckley, 2019, Buckley et al., 2011, Cowan, 1972). Hence, the two feedback mechanisms suggest a two-phase response of stomata, consisting of a hydropassive step originating from the epidermis (Buckley et al., 2011, Haworth et al., 2023, Yaaran et al., 2019, Zhang et al., 2022), followed by a hydroactive response, where ABA biosynthesis closes the stomata (McAdam et al., 2016, Yaaran et al., 2017, Sussmilch et al., 2019). Therefore, through the first step (hydropassive step), the opening of stomata occurs due to the mechanical pulling force from pavement cells towards the guard cells after a decline in water potential (Buckley, 2019). Understandably, this mechanical explanation of WWR relies on physical properties of guard cells and pavement cells such as pavement cells' geometry, stomata size, and stomata density (Haworth et al., 2021, Kwon and Choi, 2014, Powles et al., 2006, Yaaran et al., 2017, Yaaran et al., 2019). Therefore, linking anatomical features of epidermal cells to the dynamics of the stomatal responses can clarify how physical properties of the epidermal cells affect transient stomatal responses.

The formation of puzzle-like pavement cells is a complex pathway which involves cell wall components such as cellulose and pectin (Majda et al., 2017, Rongpipi et al., 2019), phytohormones such as auxin (Grones et al., 2020), and cortical microtubules (Smith, 2003). It is noticeable that some of the mechanisms that plants implement to increase drought resistance leads to the alteration of pavement cells' shape for instance. Augustine and colleagues (2015) found the overexpression of HSP70 in sugarcane (Saccharum spp. hybrid) under the drought stress which was associated to the higher cell interdigitation (Augustine et al., 2015) or the overexpression of microtubule-associated protein (AtMPB2C) showed to be involved in enhanced drought resistance and deformation of pavement cells' shape and different stomata patterning (Ruggenthaler et al., 2009). It has been speculated that higher interdigitation leads to increased cell stiffness which eventually delivers higher resistance against mechanical stresses

(Liu et al., 2021).

Two significant features of stomata, i.e. stomata density and size, have been studied massively and showed to be the key players in plants' responses to drought. A reduction in stomata density has been observed under high CO_2 concentrations and low light intensity and, in opposite, under low CO_2 concentration and high light intensity, stomata density arises (Tominaga et al., 2018). Meanwhile, higher stomata density coupled with smaller stomata is associated with higher stomata conductance, although these are not the only factors affecting stomata conductance (Bertolino et al., 2019). Smaller cells have a higher cell surface area to volume ratio, and this trait has been shown to be responsible for faster responses to osmotic changes (Drake et al., 2013, Giday et al., 2013, Kardiman and Rabild, 2017, Nunes et al., 2020). On the hand, it has been shown that the mechanical pressures change small structures less strongly than bigger structures (Sapala et al., 2018).

We set out to investigate the kinetics of the WWR in five Arabidopsis cell lines with contrasting anatomical features in the epidermis. The different genotypes differ in stomatal length, stomatal density, and in anatomical features of pavement cells (such as area, circularity, number of lobes, etc.). We hypothesized that genotypes with smaller pavement cells and stomata are more resistant against fluctuations in turgor pressure caused by any perturbation in water potential. We tested if the pavement cells with higher interdigitation have higher resistance against mechanical pressures such as turgor. The genotypes with contrasting stomata density and size allowed us to investigate mutual effects of stomata density and size on WWR.

Material and Methods

Plant material and growth conditions

Seeds of *A. thaliana* lines Col8 (Wild Type), *lcd1-1*, *epf1epf2*, UBP15-overexpression, SALK_069127 were provided from NASC (The Nottingham Arabidopsis Stock Centre). In this study, to simplify the names, UBP15-overexpression will be referred to as UBP, and SALK_069127 as SALK069. The phenotypic traits of the different lines used are described in Table 1.

Table 1- The phenotypic traits of *A. thaliana* genotypes used in this study (NASC, 1991)

Genotype	NASC catalog number	Notes
Col-8	N60000	Background: Col-0
epf1epf2	N67139	Higher stomata density and smaller stomata than col8, SALK069, *lcd1-1*, and UBP. Stomata are visible in clusters.
lcd1-1	N6359	Palisade parenchyma showed lower cell density; therefore, the whole plant looks pale green. Higher stomata density than Col8, and UBP with smaller stomata than Col8, SALK069, and UBP. The size of the stomata is similar to *epf1epf2*.
SALK_069127	N569127	Due to higher ABA accumulation in seeds, seeds need stratification before sowing. The whole plant looks larger than

		Col8 with larger leave. Higher stomata density and smaller stomata than Col8.
UBP15-overexpression	N70771	The main feature of UBP is the large stomata, epidermal and mesophyll cells than Col8.

14 plants per genotype were grown in individual pots of (diameter =13 cm) containing 50 % potting soil (Kranzinger GmbH, Austria), 33 % quartz sand, and 17 % perlite. Plants were grown for five weeks in a growth room (Walk-in FytoScope, Conviron MTPS 120, Manitoba, Canada) with a 16 h photoperiod and the following settings: day/night temperature 22/18 °C, 60-65 % humidity (RH), and 130-150 µmol m^{-2} s^{-1} light intensity. Only well-grown and fully expanded leaves were used for further analysis (described below).

Gas exchange measurements and WWR experiments

The plants were watered daily for a cultivation period of six weeks. The stomatal conductance to water vapor (g_{sw}) was measured using a portable photosynthesis system (LI-6800, LI-COR Biosciences, Lincoln, NE). The leaf temperature inside the chamber was maintained at 25 °C along with a saturating light level of 400 µmol m^{-2} s^{-1} and a reference CO_2 concentration of 400 µmol mol^{-1}. The humidity of the air entering the leaf chamber was set to 20 mmol mol^{-1}, which corresponded to a relative humidity of 64% (hereafter called "high RH"), close to the RH of the growth room. Before logging the data, leaves acclimated to these conditions for 10-15 minutes to reach a steady state. We defined the steady state as no variations in g_{sw} more than ± 0.1 (n = 600 measurements) for 5-10 minutes. Subsequently, the humidity was reduced to 5 mmol mol^{-1} (corresponding to 16% RH, hereafter called "low RH"). After again reaching a steady state at this lower RH, the humidity was elevated back to the high RH and left to acclimate. To study epidermal anatomy, seven leaves were labelled and put aside for a subsequent microscopic analysis (see below). The other seven leaves were kept in the gas-exchange chamber, but the petiole of the remaining 6 leaves was cut using a razor blade just below the lamina, to separate the leaf from the plant (called "excision" hereafter). Further gas-exchange data was recorded for 20-30 minutes.

After changing the humidity in the leaf chamber, the water differential in the chamber becomes unstable. To account for this effect, the same protocol was performed without a leaf, and the time of disruption in measurements was recorded. The test with the empty chamber, showed that the recorded measurements 1-2 minutes after reducing the humidity are due to air turbulences caused by humidity shift and were excluded from the measurements.

The kinetics of the WWR

The kinetics of the WWR were analyzed using gsw values extracted at specific time point, following Buckley et al (2011). During the change from high to low RH, time 1 (T1) represents the steady_state gsw before switching to low RH (g1), time 2 (T2) is when gsw reached its maximum during the WWR (g2), and time 3 (T3) is when gsw returned to the g_1 value (g3).

Time (T_4) is the steady state gsw and the time of petiole excision (g4), time 5 (T5) is gsw at peak WWR (g5), and time 6 (T6) is when gsw reached back g4. The kinetics of WWR were described by the size (S), length (L), and rate (V=S/L) based on Buckley et al (2011). The size of the WWR represents how large stomata conductance increased after humidity reduction/leaf excision and WWR length represents how long it took to reach the maximum stomata conductance after humidity reduction/leaf excision. Size of the WWR during a shift from high to low RH (S_h) was calculated as $g_2 - g_1$, while WWR length (L_h) was calculated as $T_2 - T_1$ and its rate of the opening (V_h) as S_h/L_h. Accordingly, the size and length of the WWR following petiole excision was calculated as $S_e = g_5 - g_4$ and $L_e = T_5 - T_4$, respectively, and the rate of the opening as $V_e = S_e/L_e$.
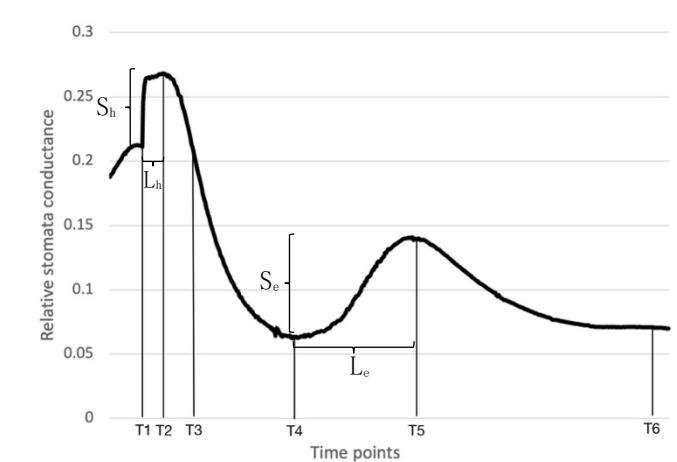

Figure 1- Schematic image of the relative stomatal conductance in response to a reduction in humidity at timepoints T0 to T6. T0 is the start of recording the measurements. T_1 indicates the humidity reduction to 10 mmol mol^{-1}. At T_2, g_{sw} reached its highest value. At T_3, g_{sw} dropped back to the value of g_{sw} at T_1. At T_4, the leaf was excised. The highest g_{sw} occurred at T_5 after cutting the leaf. S_e At T_6, g_{sw} reached back to T_4. S_h: WWR size caused by reducing the humidity, L_h: WWR length caused by reducing the humidity, S_e: WWR size caused by excision, and L_e: WWR length caused excision.

Stomata density and stomata length

To extract the features of the epidermal cells, detailed images of the epidermis were collected by Scanning Electron Microscopy (SEM). A method based on Talbot and White (Talbot and White, 2013) was adapted, with methanol fixation and dehydration in ethanol for best preservation of the cell morphology. Mature leaves were fixed in 100 % methanol for 10 minutes, followed by two dehydration steps in 100 % ethanol for 30 minutes. Critical point drying (Leica, CPD300) was performed based on the manufacturer's protocol(CPD300, 2012). Two small and flat pieces of three leaves were cut and one piece of abaxial surface and one piece of adaxial surface were mounted on stubs using double sticky carbon tape. Since the imaging was performed under high vacuum, the samples were coated with gold. Three images at different sites of abaxial and adaxial surface were acquired by SEM (JEOL IT300). On each

image, three individual squares (5000 x 5000 µm) were selected to count the number of stomata. Stomata density (SD). The stomata length (SL) was calculated by averaging the length of 30 stomatal apertures (Savvides et al., 2011), measured in ImageJ (Schneider et al. 2012).

Extraction of epidermal cell features

To extract features of pavement cells, the images provided by SEM were analyzed using the PaCeQuant plugin of Fiji/ImageJ (Möller et al., 2017). Since the plugin requires high-contrast images, cell boundaries were manually highlighted in GIMP-2.10 (The GIMP Development Team, 2019) and added to the image as a second layer which was used in PaCeQuant. Based on Sapala et al (2019), six features were selected to quantify the anatomy of the pavement cells: cell area, which describes the projected surface area of the cell, circularity is a measure of how close the cell shape is to a perfect circle, branch length indicates the length of the cell branches, longest path length is the distance between the two furthest points within the cell, convexity describes the magnitude of indentations (Sapala et al., 2019), and cell lobes indicates the number of lobes along the cell contour (Möller et al., 2017). The workflow of the feature extraction is illustrated in figure 2.
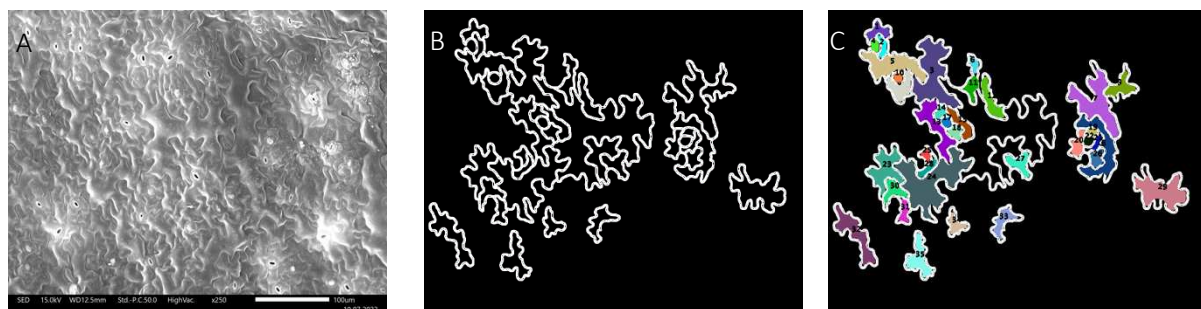

Figure 2- The workflow of hand segmentation and epidermal cell feature extraction with PaCeQuant. A) Original image taken by SEM. B) Hand-segmentation and highlighted cell boundaries. C) Extraction of pavement cell features provided by PaCeQuant labeled with colors and numbers.

Statistical analysis

The normality of the data was tested with the Shapiro–Wilk test which revealed non_normal distribution for all data sets except SS. Therefore, for statistical analysis of non_normal distributed data, the nonparametric Kruskal-Wallis test was applied in R package (2023.09.0), which is the equivalent of the parametric one-way ANOVA which was conducted for the SS data. In this study, the Kruskal-Wallis and one-way ANOVA tests tested the null hypothesis implying that the studied genotypes are not significantly different regarding SD, SS, pavement cells' features, and WWR parameters. In further, the Dunnett's test was addressed in the R package (2023.09.0) as the post hoc test.

The linear regression was applied in R package (2023.09.0) to show the linear relationship between the dependent variable Y (WWR parameters) and a single independent variable X (SD, SS, and pavement cells 'features) by the equation $Y = a + bX$, where a represents the y-intersect

of the line, b is its slope, and Y and X represent Y and X coordinates, respectively.

Results

Stomata density (SD) and stomata size (SS)

The number of stomata per unit leaf area in the different genotypes of *A. thaliana* (stomatal density, SD) is shown in figure 3.

In abaxial surface, *epf1epf2* exhibited the highest number of stomata (438 mm^{-2}) than all the other genotypes (52%, 50%, 53%, and 44% higher than Col8, SALK069, UBP, and *lcd1-1*, respectively, $p < 0.0001$). Moreover, *lcd1-1* (246 mm^{-2}) showed significantly higher SD than Col8 (206 mm^{-2}, 15% higher, $p<0.01$) and UBP (204 mm^{-2}, 16% higher, $p<0.01$). The SD was not significantly different between Col8, UBP and SALK069 (216 mm^{-2}).

In adaxial surface, *epf1epf2* (368 mm^{-2}) has more stomata compared to Col8 (157 mm^{-2}), SALK069 (194 mm^{-2}), UBP (180 mm^{-2}), and *lcd1-1* (207 mm^{-2}) by 57%, 47%, 51%, and 43%, respectively ($p<0.0001$). *lcd1-1* showed significantly higher SD in adaxial surface than Col8 (by 25%, $p<0.001$). Col8 had the lower SD than *epf1epf2*, *lcd1-1*, SALK069, and UBP number of stomata ($p < 0.0001$, $p<0.001$, $p<0.001$, $p<0.01$, respectively) and there was no significant difference between UBP and SALK069.

In total, *epf1epf2* exhibited the highest SD (807 mm^{-2}) compared to other genotypes (55%, 49%, 52%, and 44% higher than Col8, SALK069, UBP, and *lcd1-1*, respectively, $p<0.0001$). *lcd1-1* (452 mm^{-2}) showed significantly higher SD than Col8 (363 mm^{-2}, 20% higher, $p<0.001$) and UBP (383 mm^{-2}, 15% higher, $p<0.01$). SALK069 (410 mm^{-2}) showed significantly higher SD than Col8 by 11% ($p<0.01$). There was no significant difference between Col8 and UBP as well as between SALK069 and *lcd1-1*.

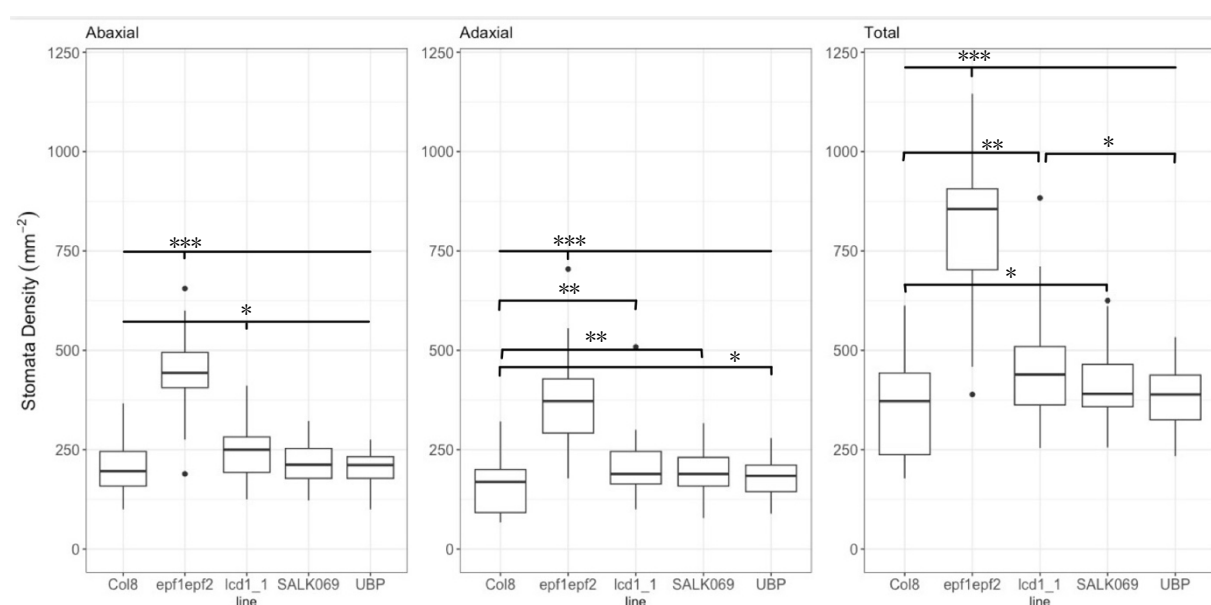

Figure 3- The variation of stomata density between the genotypes. The SD in abaxial surface, adaxial surface, and in total. Number of measurements: n = 21

The length of the stomatal aperture was measured and shown in Figure 4 (Savvides et al., 2011). In abaxial surface, UBP showed the largest SS (20.6 μm) and *lcd1-1* (19.4 μm) showed the smallest SS (p<0.0001). There was no significant difference between Col8, *epf1epf2*, and SALK069.

In adaxial surface, UBP and Col8 showed the largest SS (20.50μm and 20.12 μm, respectively. P<0.0001) and *epf1epf2*, *lcd1-1*, and SALK069 (18.6, 19, and 19.42μm) showed the smallest SS (p<0.0001).

The average length of the stomata showed that UBP developed the largest SS (20.54 μm, P<0.0001) than all genotypes. Meanwhile Col8 (20.01 μm) had the larger stomata aperture than *epf1epf2* (19.32 μm, p<0.0001), *lcd1-1* (19.24 μm), and SALK069 (19.64 μm) (p<0.0001). *epf1epf2* and *lcd1-1* showed the smallest SS (19.32 and 19.24 μm, respectively. p<0.0001). SS was not significantly different between *epf1epf2* and *lcd1-1* (Fig. 4).
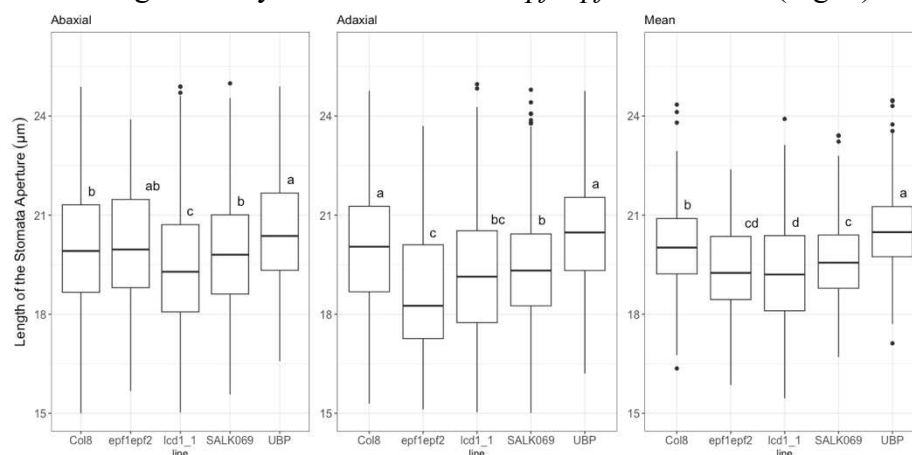

Figure 4- Stomata size calculated based on the length of the guard cells. UBP and Col8 showed the largest stomata while *epf1epf2* and *lcd1-1* showed smallest SS in average. Number of measurements: n= 300

Features of pavement cells

The main features defining the pavement cells' anatomy (Fig.5B) (Sapala et al., 2019) extracted from SEM images and analyzed in PaCeQuant plugin (Fig.5A).

In abaxial surface, *epf1epf2* showed a significantly smaller cell area than Col8, *lcd1-1*, SALK069, and UBP (by 68% (p<0.0001), 53% (p<0.01), 55% p<0.001, and 66% (p<0.0001), respectively). Col8 showed larger cell area than *lcd1-1* and SALK069 (by 31% (p<0.001) and 28% (p<0.01), respectively) but it was not different than that in UBP. The cell area was also not different between SALK069 and *lcd1-1*. *epf1epf2* showed significantly larger cell circularity than all other genotypes (24% more than Col8 and *lcd1-1* (p<0.0001), 20% than SALK069 (p<0.001) and 22% than UBP (p<0.001)). epf1epf also showed larger branch lengths than Col8 and UBP (by 26% (p<0.001) and 16% (p<0.0001), respectively). *epf1epf2* showed significantly smaller path length than all tested genotypes (49% less than Col8, 40% than SALK069, 47% than UBP, and 39% than *lcd1-1*. p<0.001). Col8 had larger path lengths than *lcd1-1* by 12% as well (p<0.01). *epf1epf2* had the biggest cell convexity by 9%, 6%, 6%, and 7% when compared

to Col8, SALK069, and *lcd1-1*, respectively (p<0.0001). *epf1epf2* had a smaller lobe count than Col8 by 52%, SALK069 by 44%, UBP by 48%, and *lcd1-1* by 45% (p<0.0001).

In the adaxial surface, *epf1epf2* was significantly different than Col8, *lcd1-1*, SALK069, and UBP by having 36% (p<0.01), 33% (p<0.01), and 20% (p<0.05), and 20% (p<0.05) smaller cell area, respectively. *epf1epf2* showed larger cell circularity than Col8, SALK069, UBP, and *lcd1-1* (by 20% (p<0.0001), 15% (p<0.001), 15%(p<0.001), and 11%(p<0.001), respectively). There was no significant different between the genotypes regarding branch length. *epf1epf2* also showed smaller path length than Col8, *lcd1-1*, SALK069, and UBP (31% (p<0.01), 26% (p<0.01), 27% (p<0.01), and 25% (p<0.01), respectively). The cell convexity was significantly larger in *epf1epf2* than Col8, SALK069, and UBP (by 7%, 4%, and 4%, respectively). *epf1epf2* had the significant lower lobe count than other genotypes (by 37%, 35%, 36%, and 33% than Col8, SALK060, UBP, and *lcd1-1*. (p<0.0001)) (Fig. 5C).

Moreover, the anatomical variation between abaxial and adaxial surface was calculated. The longest path length of epidermal cells was not significantly different between abaxial and adaxial surface in any lines. The cell circularity was significantly different in all lines between abaxial to adaxial surface. The largest difference of cell circularity between abaxial and adaxial surface was observed in *epf1epf2* (p<0.0001), *lcd1-1* (p<0.0001), and SALK069 (p<0.0001) followed by Col8 (p<0.01) and UBP (p<0.001). The difference in branch length between abaxial and adaxial surfaces was significant in *epf1epf2* (p<0.0001), *lcd1-1* (p<0.0001), and SALK069 (p<0.001) by 32%, 38%, and 27%. All lines showed a significant difference between abaxial and adaxial surface regarding the cell convexity. *epf1epf2* showed the smallest different convexity between abaxial to adaxial surface (3%, (p<0.001)) followed by Col8 (p<0.01), SALK069 (p<0.001) and UBP (p<0.01) by 5% and 4%, respectively. *lcd1-1* showed the largest different cell convexity between abaxial and adaxial surface by 7% p<0.0001). The lobe count was significantly different between abaxial and adaxial surface in Col8 and UBP by 23% and 17% p<0.01) (Fig. 5C).
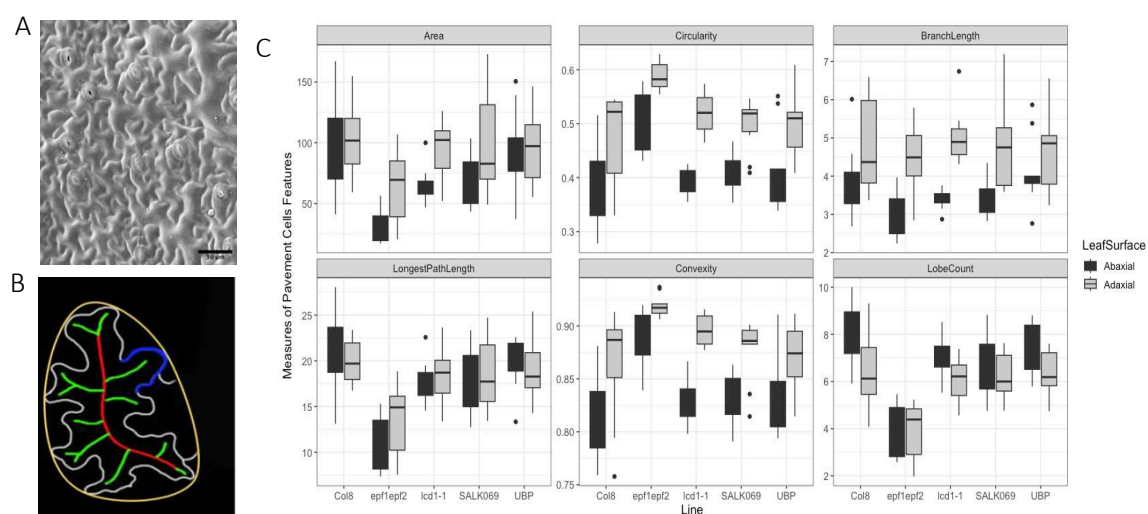
Figure 5- Anatomical characteristics of epidermal cells. A) SEM image of the epidermis. B) pavement cells' features explaining the anatomy of the pavement cells including perimeter (white line), convexity (yellow line), skeleton consisting of longest path length (red line) and average branch length (green lines), and lobe counts (blue line). C) Anatomical characteristics of epidermal cells in abaxial and adaxial surfaces in the five genotypes of *A. thaliana*. Number of measurements: n =21

WWR parameters

WWR parameters were calculated based on fluctuations in g_{sw} after a decline in water potential. Figure 6 shows the temporal fluctuations in g_{sw} after humidity reduction (T1) and leaf excision (T4). The occurrence of the WWR has been defined as an increase in g_{sw} after humidity reduction (T2) or leaf excision (T5).

Col8 showed significantly larger S_h (0.5) than *epf1epf2* (0.28, p<0.001), *lcd1-1* (0.26, p<0.001), and SALK069 (0.30, p<0.001,) followed by UBP (0.44) which showed significantly larger S_h than *epf1epf2* (p<0.01), *lcd1-1*(p<0.01), and SALK069 (p<0.01) (Fig. 6A). L_h was not significantly different between the genotypes (Fig. 6B). Accordingly, V_h in Col8 (872.6, p<0.01) and UBP (838.16, p<0.01) was significantly larger than *epf1epf2* (488.6, p<0.01), *lcd1-1* (495.45, p<0.01), and SALK069 (538.98, p<0.01) by ~ 41%, 40%, and 35%, respectively (Fig. 6C).

After leaf excision, S_e and L_e showed to be significantly lower in *epf1epf2* (0.007 and 0.0004, p<0.0001) than all the other genotypes (Fig. 6D and E). *epf1epf2* showed significantly smaller V_e (19.29) than Col8 (103.21, p<0.001), *lcd1-1* (47.64, p<0.05), UBP (98.28, p<0.01), and SALK069 (100.22, p<0.01) (Fig. 6F).
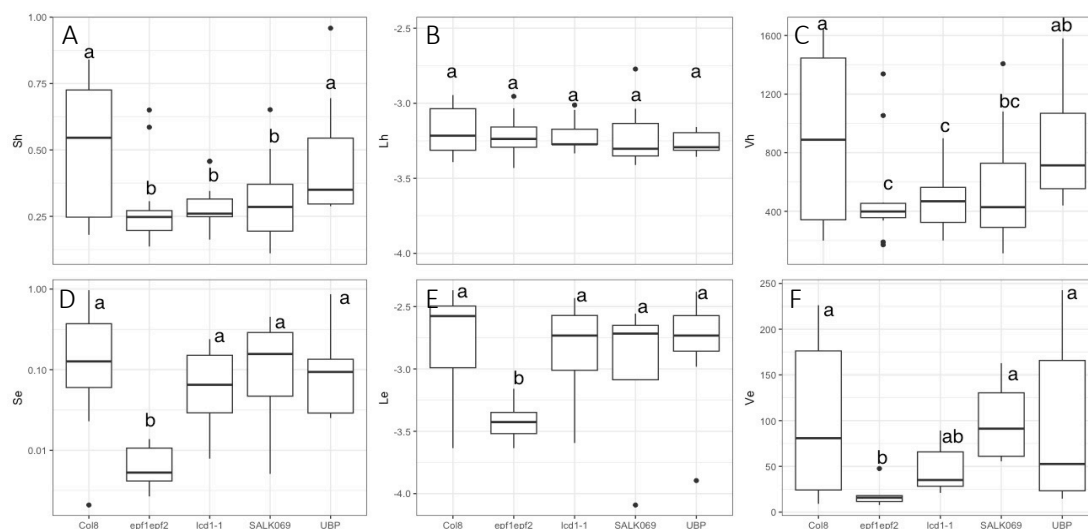

Figure 6- WWR parameters in respond to humidity reduction and leaf excision. A) Size of the WWR triggered by reduced air humidity (S_h). B) Length of the WWR triggered by reduced air humidity (L_h). C) Rate of the WWR triggered by reduced air humidity (V_h). D) Size of the WWR triggered by leaf excision (S_e) E) Length of the WWR triggered by leaf excision (L_e). F) Rate of the WWR triggered by leaf excision (V_e). Number of measurements for low humidity: 14 leaves

The linear model regressions

The linear regression showed a significant and negative correlation between size of the epidermal cells (both stomata ($R2= 0.77$, $p= 0.05$, Fig. 7B), while the linear model did not show any correlation between SD and V_h ($R2= 0.36$, $p= 0.2$, Fig.7A). In the present work, cell area, branch length and the longest path length represented the size of the cells while lobe count, circularity and convexity showed the shape of the pavement cells (Sapala et al., 2019). According to the linear models, a decreasing size of epidermal cell in abaxial surface was linked to the decreasing V_h (Fig. 8A-C). While there was a correlation between Vh and SD ($R2=0.78$, $p= 0.04$, Fig. 9A), the linear model did not show a correlation between SS and V_e ($R2= 0.55$, $p=0.14$, Fig. 9B). Similar to when humidity was reduced, the linear regression showed a significant and negative correlation between the size of the pavement cells' in abaxial surface and V_e (Fig. 10A-C).
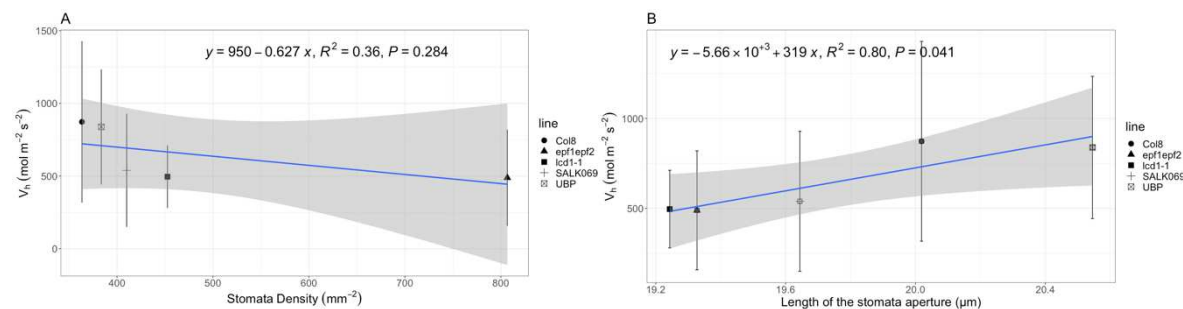

Figure 7- Linear models describing the rate of stomata transient opening triggered by reduced humidity (V_h) along with increasing A) SD and B) SS.
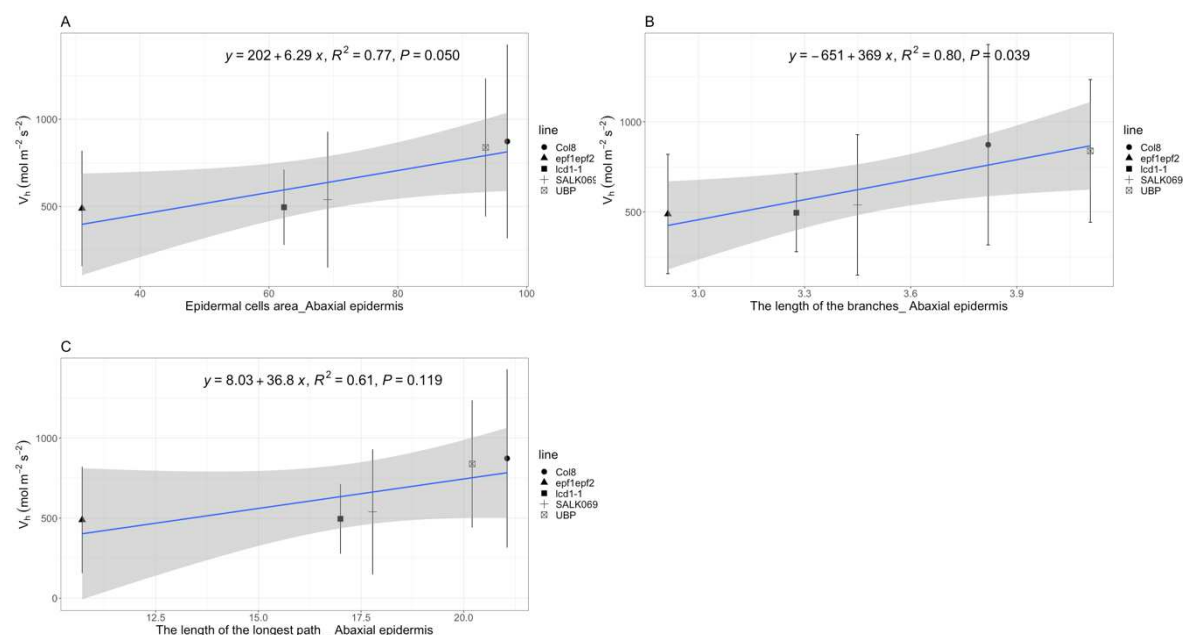

Figure 8- the linear models describing the rate of stomata transient opening triggered by reduced humidity (V_h) along with increasing A) cell area, B) branch length, and C) longest path length.
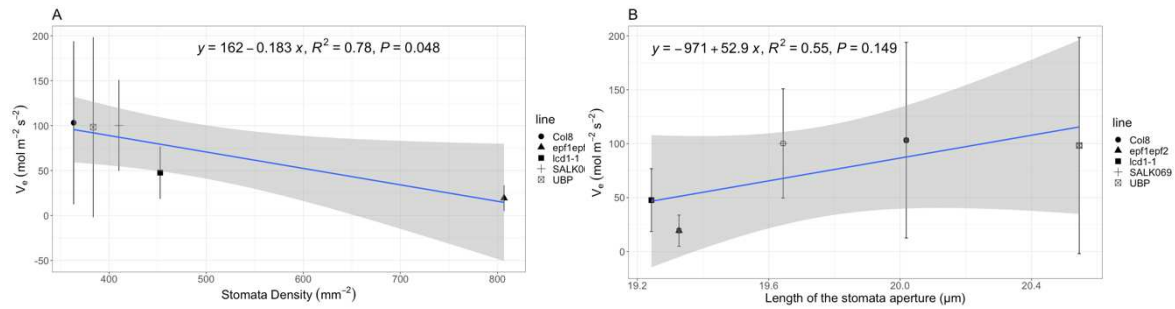
Figure 9- Linear models describing the rate of stomata transient opening triggered by leaf excision (V_e) along with increasing A) SD and B) SS.
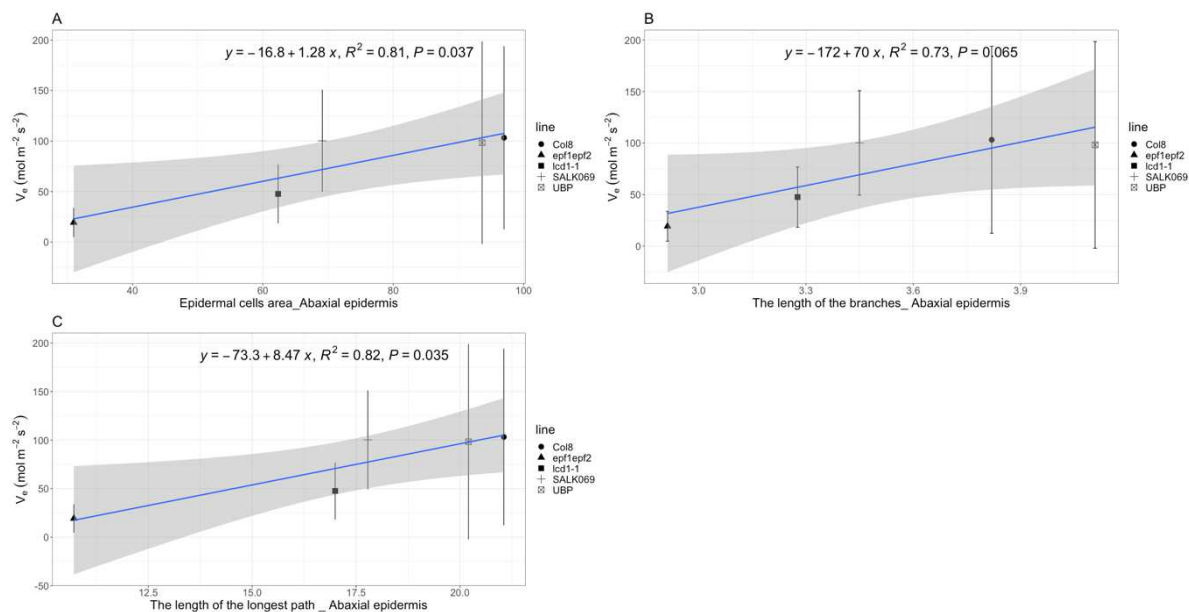

Figure 10- the linear models describing the rate of stomata transient opening triggered by leaf excision (V_e) along with increasing A) cells' area, B) branch length, and C) longest path length.

Discussion

In this work, we have observed a biphasic stomata response to a drop in water potential triggered either by a switch from high to low air humidity or by leaf excision. The transient opening of stomata, immediately after a drop in water potential and the subsequent stomata closure has been reported previously (Buckley, 2005, Buckley et al., 2011, Hsu et al., 2021, Kwon and Choi, 2014, Westbrook and McAdam, 2021). The most accepted hypothesis explaining the WWR suggests a passive and non-ABA dependent pathway after a decrease in water potential, through which the turgor pressure of the pavement cells decline and pull the guard cells which resulted in transient opening of stomata (Buckley, 2019). The observations in our work implied that in response to the reduced air humidity, Col8 and UBP showed significantly larger V_h than *epf1epf2*, *lcd1-1*, and SALK069. L_h was not different between the genotypes which illustrated that the higher V_h in Col8 and UBP is caused by larger stomata opening (larger S_h) than in *epf1epf2*, *lcd1-1*, and SALK069. According to the linear models, the V_h in studied genotypes is correlated to the size of the pavement cells (Fig. 8A-C) and stomata (Fig.7B) while SD did not explain different V_h. Bassel and colleagues (2014) showed that when comparably small and

large cells are under the same pressure, the larger cells 'expand' more than smaller ones. They suggested that there is a mechanical advantage for small cells to alleviate the mechanical stress caused by turgor pressure (Bassel et al., 2014). Through finite element modeling, Sapala et al (2018) proposed the higher cells' interdigitation or lower cell size as the two mechanisms that plants adapt to confront the mechanical stresses (Sapala et al., 2018). Accordingly, our linear models showed that the smaller V_h is correlated to the smaller epidermal cell in abaxial epidermis (Fig. 8A-C). It is worth to mention here that the general idea stating that small cells have faster ion exchange due to the higher cell surface area to volume ratio, does not explain the observed lower V_h since this idea implies faster movement of small cells which means smaller L_h in genotypes with comparably smaller cells. However, we did not observe any difference in L_h between the genotypes. Consequently, it is concluded that the small epidermal cells experienced less mechanical stress after the decline in water potential caused by reduced air humidity, therefore at the time that hydroactive response initiates to close stomata (which took the same time interval in all genotypes), the genotypes with comparably smaller epidermal cells showed already smaller transient opening (S_h).

Interestingly and opposite to V_h, there was no correlation between SS and V_e (Fig. 9B). In response to the leaf excision, *epf1epf2* showed significantly smaller V_e than Col8, *lcd1-1*, UBP, and SALK069. Since, opposite to L_h, epf1pef2 showed significantly lower L_e than other genotypes (Fig. 6E), it seems that the higher stomata conductance caused by higher SD (Franks and Beerling, 2009, Haworth et al., 2021, Sakoda et al., 2020) in *epf1epf2* (with ~50% higher SD than other genotypes) altered the inner leaf air e.g. its temperature and humidity faster than in the other genotypes, which ultimately triggers the hydroactive response earlier (Bharath et al., 2021, McAdam et al., 2016, Merilo et al., 2014, Merilo et al., 2017). This explanation supports the idea that stomata rather respond to gradient changes in intercellular air spaces not to the ambient factors such as air humidity (Baillie and Fleming, 2020, Buckley, 2019, Harrison et al., 2020, Mott, 1988, Tominaga et al., 2018, Wall et al., 2022). Accordingly, the higher SD has been suggested as an evolutionary feature in vascular plants to deliver an optimum photosynthesis rate (Westbrook and McAdam, 2021). Nevertheless, there is a dilemma about how SD was not correlated to V_h while it is negatively correlated to V_e (Fig. 9A) and how higher SD in *epf1epf2* did not stimulate faster stomata closure when air humidity was reduced. The explanation could reside in the difference between S_h and S_e, meaning that after air humidity reduction stomata opened sufficiently large enough to trigger the hydroactive response, while after the leaf excision, where stomata opened comparably smaller, a greater number of stomata are needed to initiate a hydroactive response. The correlation between decreasing size of the pavement cells and smaller V_e (Fig. 10A-C) suggests that the size, rather than the shape of the pavement cells, drives the WWR dynamics triggered by either reduced air humidity or leaf excision.

The WWR rates were only correlated to the size of the pavement cells in abaxial surface (Fig.8 and 10). According to Wall et all (2022), the two leaf surfaces 'act independently' because the

observed changes in stomatal conductance in abaxial surface did not affect stomata responses in the adaxial surface (Wall et al., 2022). The structure of the spongy mesophyll close to the abaxial surface, which inevitably necessitates different signal transduction pathways for stomata movement, has been suggested as a cause of a higher stomata sensitivity to environmental factors (Paradiso et al., 2020, Wang et al., 2008, Zhang et al., 2016). Accordingly, experiments on epidermal peals (isolated from the mesophyll) revealed faster stomata responses in adaxial surface than in abaxial surface (Pemadasa, 1982). Nevertheless, there is not much data about how the anatomy of the pavement cells in abaxial surface differentiates from those in adaxial surface after environmental fluctuations. In this work, the genotypes of *A. thaliana* with smallest pavement cells in abaxial surface had the smallest stomatal transient opening. Our interpretation is that the higher number of stomata in abaxial surface initially forms smaller pavement cells and contributes to the smaller WWR response in corresponding genotypes.

The present findings agree with previous studies which explain the relation between anatomical properties of leaves and plant physiological responses. Plants belonging to Marsileaceae, with similar photosynthetic rate like gymnosperms, showed WWR induced by leaf excision which was correlated to the higher SD than other ferns (Westbrook and McAdam, 2021). In the latter study, the size of stomata aperture has not been evaluated however, the opposing relation between SD and SS may provide more holistic view (Caine et al., 2023, Qie et al., 2023).The inverse relation between SD and SS (i.e. plants with higher number of smaller stomata) has been reported as an anatomical privilege to increase drought resilience (Drake et al., 2013) and improve WUE (Caine et al., 2023) under environmental stresses (Haworth et al., 2023). We observed a slighter stomatal transient opening in an epidermis with smaller stomata and abaxial pavement cells which implies that small cells are more resilient to volume changes under mechanical stresses. This finding favors the idea of higher capability of small structures to adjust their anatomy to confront mechanical stresses (Caine et al., 2023, Drake et al., 2013, Kardiman and Rabild, 2017, Théroux-Rancourt et al., 2021). Moreover, the higher SD initiated an earlier hydroactive response which resulted in shorter transient opening. Nevertheless, as we discussed before, stomata responses are affected by more than just the epidermis, and the physical properties of mesophyll should not be overlooked. Therefore, follow-up studies on the anatomical properties of mesophyll in plants with varying WWR kinetics are suggested and to incorporate them to the fundings of this work in order to generate a more holistic view of the dynamics of stomatal transient opening.

Acknowledgement

References

AUGUSTINE, S. M., CHERIAN, A. V., SYAMALADEVI, D. P. & SUBRAMONIAN, N. 2015. Erianthus arundinaceus HSP70 (EaHSP70) Acts as a Key Regulator in the Formation of Anisotropic Interdigitation in Sugarcane (Saccharum spp. hybrid) in Response to Drought Stress. *Plant and Cell Physiology,* 56**,** 2368-2380.

BAILLIE, A. L. & FLEMING, A. J. 2020. The developmental relationship between stomata and mesophyll airspace. *New Phytologist,* 225**,** 1120-1126.

BASSEL, G. W., STAMM, P., MOSCA, G., BARBIER DE REUILLE, P., GIBBS, D. J., WINTER, R., JANKA, A., HOLDSWORTH, M. J. & SMITH, R. S. 2014. Mechanical constraints imposed by 3D cellular geometry and arrangement modulate growth patterns in the *Arabidopsis* embryo. *Proceedings of the National Academy of Sciences,* 111**,** 8685-8690.

BERTOLINO, L. T., CAINE, R. S. & GRAY, J. E. 2019. Impact of Stomatal Density and Morphology on Water-Use Efficiency in a Changing World. *Frontiers in Plant Science,* 10.

BHARATH, P., GAHIR, S. & RAGHAVENDRA, A. S. 2021. Abscisic Acid-Induced Stomatal Closure: An Important Component of Plant Defense Against Abiotic and Biotic Stress. *Frontiers in Plant Science,* 12.

BUCKLEY, T. N. 2005. The control of stomata by water balance. *New Phytologist,* 168**,** 275-292.

BUCKLEY, T. N. 2019. How do stomata respond to water status? *New Phytologist,* 224**,** 21-36.

BUCKLEY, T. N., SACK, L. & GILBERT, M. E. 2011. The Role of Bundle Sheath Extensions and Life Form in Stomatal Responses to Leaf Water Status *Plant Physiology,* 156**,** 962-973.

CAINE, R. S., HARRISON, E. L., SLOAN, J., FLIS, P. M., FISCHER, S., KHAN, M. S., NGUYEN, P. T., NGUYEN, L. T., GRAY, J. E. & CROFT, H. 2023. The influences of stomatal size and density on rice abiotic stress resilience. *New Phytologist,* 237**,** 2180-2195.

COWAN, I. R. 1972. Oscillations in stomatal conductance and plant functioning associated with stomatal conductance: Observations and a model. *Planta,* 106**,** 185-219.

CPD300, O. M. 2012. Leica Microsystem, Vienna, Austria.

DARWIN, F. 1898. Observations on stomata. *Proceedings of the Royal Society of London,* 63**,** 413-417.

DRAKE, P. L., FROEND, R. H. & FRANKS, P. J. 2013. Smaller, faster stomata: scaling of stomatal size, rate of response, and stomatal conductance. *J Exp Bot,* 64**,** 495-505.

FRANKS, P. J. & BEERLING, D. J. 2009. Maximum leaf conductance driven by CO_2 effects on stomatal size and density over geologic time. *Proceedings of the National Academy of Sciences,* 106**,** 10343-10347.

GIDAY, H., KJAER, K. H., FANOURAKIS, D. & OTTOSEN, C.-O. 2013. Smaller stomata require less severe leaf drying to close: A case study in Rosa hydrida. *Journal of Plant Physiology,* 170**,** 1309-1316.

GRONES, P., MAJDA, M., DOYLE, S. M., VAN DAMME, D. & ROBERT, S. 2020. Fluctuating auxin response gradients determine pavement cell-shape acquisition. *Proceedings of the National Academy of Sciences,* 117**,** 16027-16034.

HARRISON, E. L., ARCE CUBAS, L., GRAY, J. E. & HEPWORTH, C. 2020. The influence of stomatal morphology and distribution on photosynthetic gas exchange. *The Plant Journal,* 101**,** 768-779.

HAWORTH, M., MARINO, G., LORETO, F. & CENTRITTO, M. 2021. Integrating stomatal physiology and morphology: evolution of stomatal control and development of future crops. *Oecologia,* 197**,** 867-883.

HAWORTH, M., MARINO, G., MATERASSI, A., RASCHI, A., SCUTT, C. P. & CENTRITTO, M. 2023. The functional significance of the stomatal size to density relationship: Interaction with atmospheric [CO2] and role in plant physiological behaviour. *Science of The Total Environment,* 863**,** 160908.

HSU, P.-K., TAKAHASHI, Y., MERILO, E., COSTA, A., ZHANG, L., KERNIG, K., LEE, K. H. & SCHROEDER, J. I. 2021. Raf-like kinases and receptor-like (pseudo)kinase GHR1 are required for stomatal vapor pressure difference response. *Proceedings of the National Academy of Sciences,* 118**,** e2107280118.

KARDIMAN, R. & RABILD, A. 2017. Relationship between stomatal density, size and speed of opening in Sumatran rainforest species. *Tree Physiology,* 38**,** 696-705.

KWON, H. W. & CHOI, M. Y. 2014. Generalized hydromechanical model for stomatal responses to hydraulic perturbations. *Journal of Theoretical Biology,* 340**,** 119-130.

LIU, S., JOBERT, F., RAHNESHAN, Z., DOYLE, S. M. & ROBERT, S. 2021. Solving the Puzzle of Shape Regulation in Plant Epidermal Pavement Cells. *Annual Review of Plant Biology,* 72**,** 525-550.

MAJDA, M., GRONES, P., SINTORN, I.-M., VAIN, T., MILANI, P., KRUPINSKI, P., ZAGÓRSKA-MAREK, B., VIOTTI, C., JÖNSSON, H., MELLEROWICZ, E. J., HAMANT, O. & ROBERT, S. 2017. Mechanochemical Polarization of Contiguous Cell Walls Shapes Plant Pavement Cells. *Developmental Cell,* 43**,** 290-304.e4.

MCADAM, S. A. M., SUSSMILCH, F. C. & BRODRIBB, T. J. 2016. Stomatal responses to vapour pressure deficit are regulated by high speed gene expression in angiosperms. *Plant, Cell & Environment,* 39**,** 485-491.

MERILO, E., JÕESAAR, I., BROSCHÉ, M. & KOLLIST, H. 2014. To open or to close: species-specific stomatal responses to simultaneously applied opposing environmental factors. *New Phytologist,* 202**,** 499-508.

MERILO, E., YARMOLINSKY, D., JALAKAS, P., PARIK, H., TULVA, I., RASULOV, B., KILK, K. & KOLLIST, H. 2017. Stomatal VPD Response: There Is More to the Story Than ABA *Plant Physiology,* 176**,** 851-864.

MÖLLER, B., POESCHL, Y., PLÖTNER, R. & BÜRSTENBINDER, K. 2017. PaCeQuant: A Tool for High-Throughput Quantification of Pavement Cell Shape Characteristics *Plant Physiology,* 175**,** 998-1017.

MOTT, K. A. 1988. Do Stomata Respond to CO_2 Concentrations Other than Intercellular? 1. *Plant Physiology,* 86**,** 200-203.

NASC 1991. The Nottingham Arabidopsis Stock Centre

NUNES, T. D. G., ZHANG, D. & RAISSIG, M. T. 2020. Form, development and function of grass stomata. *Plant J,* 101**,** 780-799.

PARADISO, R., DE VISSER, P. H. B., ARENA, C. & MARCELIS, L. F. M. 2020. Light response of photosynthesis and stomatal conductance of rose leaves in the canopy profile: the effect of lighting on the adaxial and the abaxial sides. *Functional Plant Biology,* 47**,** 639-650.

PEMADASA, M. A. 1982. DIFFERENTIAL ABAXIAL AND ADAXIAL STOMATAL RESPONSES TO INDOLE-3-ACETIC ACID IN COMMELINA COMMUNIS L. *New Phytologist,* 90**,** 209-219.

POWLES, J. E., BUCKLEY, T. N., NICOTRA, A. B. & FARQUHAR, G. D. 2006. Dynamics of stomatal water relations following leaf excision. *Plant, Cell & Environment,* 29**,** 981-992.

QIE, Y.-D., ZHANG, Q.-W., MCADAM, S. A. M. & CAO, K.-F. 2023. Stomatal dynamics are regulated by leaf hydraulic traits and guard cell anatomy in nine true mangrove species. *bioRxiv***,** 2023.02.01.526604.

RONGPIPI, S., YE, D., GOMEZ, E. D. & GOMEZ, E. W. 2019. Progress and Opportunities in the Characterization of Cellulose – An Important Regulator of Cell Wall Growth and Mechanics. *Frontiers in Plant Science,* 9.

RUGGENTHALER, P., FICHTENBAUER, D., KRASENSKY, J., JONAK, C. & WAIGMANN, E. 2009. Microtubule-associated protein AtMPB2C plays a role in organization of cortical microtubules, stomata patterning, and tobamovirus infectivity. *Plant Physiol,* 149**,** 1354-65.

SAKODA, K., YAMORI, W., SHIMADA, T., SUGANO, S. S., HARA-NISHIMURA, I. & TANAKA, Y. 2020. Higher Stomatal Density Improves Photosynthetic Induction and Biomass Production in Arabidopsis Under Fluctuating Light. *Frontiers in Plant Science,* 11.

SAPALA, A., RUNIONS, A., ROUTIER-KIERZKOWSKA, A. L., DAS GUPTA, M., HONG, L., HOFHUIS, H., VERGER, S., MOSCA, G., LI, C. B., HAY, A., HAMANT, O., ROEDER, A. H., TSIANTIS, M., PRUSINKIEWICZ, P. & SMITH, R. S. 2018. Why plants make puzzle cells, and how their shape emerges. *Elife,* 7.

SAPALA, A., RUNIONS, A. & SMITH, R. S. 2019. Mechanics, geometry and genetics of epidermal cell shape regulation: different pieces of the same puzzle. *Current Opinion in Plant Biology,* 47**,** 1-8.

SAVVIDES, A., FANOURAKIS, D. & IEPEREN, W. 2011. Co-ordination of hydraulic and stomatal conductances across light qualities in cucumber leaves. *Journal of experimental botany,* 63**,** 1135-43.

SMITH, L. G. 2003. Cytoskeletal control of plant cell shape: getting the fine points. *Current Opinion in Plant Biology,*

6, 63-73.

SUSSMILCH, F. C., ROELFSEMA, M. R. G. & HEDRICH, R. 2019. On the origins of osmotically driven stomatal movements. *New Phytologist,* 222**,** 84-90.

TALBOT, M. J. & WHITE, R. G. 2013. Methanol fixation of plant tissue for Scanning Electron Microscopy improves preservation of tissue morphology and dimensions. *Plant Methods,* 9**,** 36.

THÉROUX-RANCOURT, G., RODDY, A. B., EARLES, J. M., GILBERT, M. E., ZWIENIECKI, M. A., BOYCE, C. K., THOLEN, D., MCELRONE, A. J., SIMONIN, K. A. & BRODERSEN, C. R. 2021. Maximum CO_2 diffusion inside leaves is limited by the scaling of cell size and genome size. *Proceedings of the Royal Society B: Biological Sciences,* 288**,** 20203145.

TOMINAGA, J., SHIMADA, H. & KAWAMITSU, Y. 2018. Direct measurement of intercellular CO2 concentration in a gas-exchange system resolves overestimation using the standard method. *J Exp Bot,* 69**,** 1981-1991.

WALL, S., VIALET-CHABRAND, S., DAVEY, P., VAN RIE, J., GALLE, A., COCKRAM, J. & LAWSON, T. 2022. Stomata on the abaxial and adaxial leaf surfaces contribute differently to leaf gas exchange and photosynthesis in wheat. *New Phytologist,* 235**,** 1743-1756.

WANG, Y., NOGUCHI, K. & TERASHIMA, I. 2008. Distinct light responses of the adaxial and abaxial stomata in intact leaves of Helianthus annuus L. *Plant Cell Environ,* 31**,** 1307-16.

WESTBROOK, A. S. & MCADAM, S. A. M. 2021. Stomatal density and mechanics are critical for high productivity: insights from amphibious ferns. *New Phytologist,* 229**,** 877-889.

YAARAN, A., NEGIN, B. & MOSHELION, M. 2017. Role of guard-cell ABA in determining maximal stomatal aperture and prompt vapor-pressure-deficit response. *bioRxiv***,** 218719.

YAARAN, A., NEGIN, B. & MOSHELION, M. 2019. Role of guard-cell ABA in determining steady-state stomatal aperture and prompt vapor-pressure-deficit response. *Plant Science,* 281**,** 31-40.

ZHANG, Q., TANG, W., XIONG, Z., PENG, S. & LI, Y. 2022. Stomatal conductance in rice leaves and panicles responds differently to abscisic acid and soil drought. *Journal of Experimental Botany,* 74**,** 1551-1563.

ZHANG, Z.-S., LI, Y.-T., GAO, H.-Y., YANG, C. & MENG, Q.-W. 2016. Characterization of photosynthetic gas exchange in leaves under simulated adaxial and abaxial surfaces alternant irradiation. *Scientific Reports,* 6**,** 26963.